Experimental channel response to tectonic uplift

Jens M. Turowski, Dimitri Lague, Alain Crave, Niels Hovius

Experimental channel response to tectonic uplift

Jens M. Turowski,[1] Dimitri Lague,[2] Alain Crave,[2] and Niels Hovius[1]

Received 14 March 2005; revised 4 April 2006; accepted 1 May 2006; published 10 August 2006.

[1] We have performed a series of experiments to investigate the relationship between channel geometry and tectonic forcing in steady state landscapes at various uplift rates. The experimental setup consists of uniformly uplifted silica paste eroded by artificial rainfall. In this setup, erosional landscapes evolve by growth and amalgamation of incisions, which organize into a drainage network whose dynamics are a function of the interaction between vertical channel cutting, hillslope erosion, and sediment transport. High-precision (0.5 mm pixel size) digital elevation models were constructed using a stereogrammetric camera system. From this data, channel bed slope was found to be independent of discharge and position on the experimental surface and to increase linearly with uplift rate. Geometric parameters of the flow, such as channel width or depth, could not be observed directly during the experiments. Using laminar flow equations for the mean flow velocity, these parameters were back calculated, and relationships to the imposed substrate uplift rate were derived. Channel width, cross-sectional area, and wetted perimeter decrease with increasing uplift rate to a limit value, hydraulic radius and flow depth increase slightly, and flow velocity increases approximately linearly with increasing uplift rate. These results are qualitatively consistent with recent field surveys and highlight the importance of channel width and slope variations in accommodating channel response to variable rock uplift rates.

Citation: Turowski, J. M., D. Lague, A. Crave, and N. Hovius (2006), Experimental channel response to tectonic uplift, *J. Geophys. Res.*, *111*, F03008, doi:10.1029/2005JF000306.

1. Introduction

[2] Fluvial incision drives the evolution of erosional landscapes. As the incision rate within the channel is generally assumed to be a function of its geometry, and the landscape evolves toward a steady state in which the lowering of the terrain by erosion is equal to rock uplift, the rivers will adjust their form to the tectonic forcing. Although several recent field studies [*Harbor*, 1998; *Snyder et al.*, 2000, 2003; *Lavé and Avouac*, 2001; *Duvall et al.*, 2004; *Finnegan et al.*, 2005] made significant advances, our understanding of the relationships between channel width, depth, cross-sectional form and area, and incision rate is limited and qualitative. The quantitative assessment of these links is hard to achieve in natural geomorphic systems, where it is difficult to isolate and measure the important variables and boundary conditions, and define the state of evolution of the landscape. Physical experiments allow the study of channel processes where boundary conditions can be controlled completely and the evolution of the surface can be monitored continuously. However, can experimental findings be applied to natural landscapes? Scaled models can reproduce natural systems, provided that the appropriate dimensionless quantities are conserved. It is difficult to meet this condition in geomorphic systems, firstly because a complete list of important dimensionless numbers are not yet known, and secondly because there are inherent problems in scaling, for example due to the fundamentally different timescales of tectonic and hydraulic processes. Previous laboratory studies have either attempted to maintain a strict match between the model and natural landscapes for a single process [e.g., *Paola et al.*, 1992; *Whipple et al.*, 1998; *Roering et al.*, 2001], or used experiments with dynamics that are qualitatively similar to natural systems, regardless of the dominant process [e.g., *Czirók et al.*, 1993; *Crave et al.*, 2000; *Hasbargen and Paola*, 2000; *Pelletier*, 2002; *Lague et al.*, 2003; *Bonnet and Crave*, 2003; *Babault et al.*, 2005]. The aim of our experiments has been to investigate the scaling of channel geometry with tectonic forcing. We have used the second approach to maintain a realistic coupling between hillslopes and channels.

[3] The experimental approach was as follows: (1) The experimental area made of silica paste was raised uniformly at a constant and well-known rate to simulate tectonic forcing. (2) Surface runoff was generated with a rainfall device in order to drive drainage network formation in the silica paste by growth and amalgamation of incisions. (3) The resulting topography was digitized at regular intervals. (4) For each uplift rate the experimental topography was allowed to reach a dynamic equilibrium.

[4] Our experimental set up and protocol were developed from a study by *Lague et al.* [2003]. Early studies using the

[1] Department of Earth Sciences, University of Cambridge, Cambridge, UK.
[2] Géosciences Rennes, UMR 6118, Centre National de la Recherche Scientifique, Rennes, France.

0148-0227/06/2005JF000306

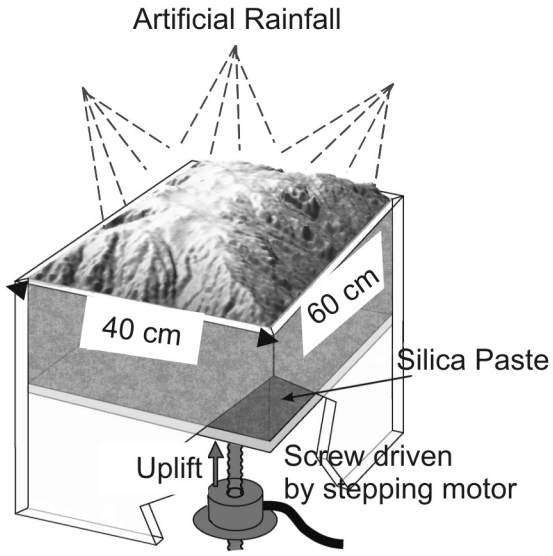

Figure 1. Experimental setup.

set up [*Crave et al.*, 2000; *Lague et al.*, 2003; *Bonnet and Crave*, 2003] did not record channelization. However, microchannels have been observed in a study using a larger experimental area [*Babault et al.*, 2005]. With this larger set up we obtained a set of channel networks that cut into uplifting material, transport the sediment produced upstream, and interact realistically with hillslopes (or more precisely the unchannelized parts of the topography), as do natural erosional channels.

[5] In the following, we present our experimental setup and methods of topographic analysis of the channels. Subsequently, we focus our analysis on the sensitivity of channel geometry to discharge and substrate uplift rate at steady state, leaving aside the analysis of the unchannelized part of the topography.

2. Setup and Methods

2.1. Facility and Material

[6] For our study, we have used a mixture of fine silica grains and water, in a box with a vertically adjustable floor, inside a rainfall simulator. A stereogrammetric camera system was used to obtain digital elevation models of the evolving experimental surface.

[7] The experimental box has a surface area of 60×40 cm^2 and a depth of 50 cm (Figure 1). The bottom of the box is moveable and can be lowered or raised at a steady rate by a step motor. The box was filled with a paste of pure silica, obtained by mixing granular silica with water in a weight ratio of 82:18. The water content was chosen such that the paste had a vertical angle of rest and infiltration was negligible. The mean grain size of the paste was 10 μm, and chemical agglomeration is thought not to affect the grain size distribution during preparation and use of the paste [cf. *Crave et al.*, 2000]. Rainfall was simulated by a system of four sprinklers positioned in the top corners of a space of $2 \times 2 \times 2$ m^3. The precipitation rate at the experimental surface can be controlled by adjusting water pressure and nozzle configuration. Uniformity of precipitation was insured as best as possible, but the maximum deviation from the mean is about 25% with a coefficient of variation of about 14%. Water droplets have a diameter below 10 μm, which is small enough to exclude grain detachment by drop impact [*Lague et al.*, 2003]. Instead, grain detachment and transport occur mainly by shear detachment through surface runoff.

[8] The topography was measured with a stereogrammetric camera system, the ATOS system by GOM (GOM France SAS, Corbeil, France), which has a precision of around 20 μm. The density of data points depends on the topography and the number of images taken. The median nearest neighbor distance was around 0.5 mm for the measurements done in this investigation. The raw data was gridded with commercial software to a pixel size of 0.5 mm and then smoothed with a median filter with a window of five pixels. Because of high droplet density in the experimental space during operation of the rainfall simulator it is not possible to observe the evolution of the experimental surface directly and the water flow has to be switched off to collect data. In previous studies it has been found that the impact of the interruption of erosion on the experimental topography is negligible [cf. *Crave et al.*, 2000].

2.2. Experimental Protocol

[9] At the start of an experiment, the material was allowed to erode for several hours (usually overnight) at a constant substrate uplift rate U until steady state was reached. This was assessed by taking digital elevation models (DEMs) and digital photographs of the surface at intervals of about half an hour until the mean elevation was constant. Then the uplift rate was increased and the process was repeated until no paste was left. We did three runs at two different precipitation rates with three or four different uplift rates each. Table 1 summarizes the conditions of the experiments. There were between 3 and 18 DEM acquisitions per uplift rate, at least two of them at steady state.

2.3. Channel Analysis

[10] Extraction of the channel parameters from the DEMs is a four-step process:

[11] 1. Catchments and cross sections within the catchments were selected. We analyzed between three and five catchments in every steady state topography, aiming for a spread of sizes and positions (Table 2). In each catchment at least six and up to twenty sections were taken perpendicular to the channel, from ridge to ridge, and at ten to fifty pixel intervals. The spacing was chosen according to the local topography and the size of the basin.

[12] 2. The discharge across a given cross section was calculated. The drainage area for every point along the cross

Table 1. Experimental Conditions[a]

Set	Precipitation Rate, mm/hr	Uplift Rates, cm/hr	Total Number of Acquisitions	Total Time Under Erosion, hours
1	45	0.75, 1.5, 2.5, R	24	~130
2	45	0.1, 0.3, 0.75, 1.25	31	86
3	140	0.1, 0.3, 0.75	31	44

[a]R refers to relaxation experiment; that is, a previously developed topography is eroded at $U = 0$.

Table 2. Number of Catchments and Channel Cross Sections Analyzed[a]

U, cm/hr	Set	Number of Catchments	Number of Sections
0.75	1	4	45
1.5	1	4	40
2.5	1	3	33
0.1	2	4	39
0.3	2	4	36
0.75	2	4	33
1.25	2	5	63
Sum		28	289

[a]The number of sections in each catchment depended on the size of the catchment and its topography.

section was calculated with a flow routing algorithm using a steepest slope criterion. Subsequently, we summed the upslope areas of all points along the cross section with an elevation of less than half a millimeter above the lowest point of the cross section, ignoring points with a contributing area of less than 10 pixels. The error due to this cutoff is small as the total area draining across a section is usually of order of 10^5 pixels in size and the flow concentrates around the thalweg. The discharge Q was calculated in two ways: (1) by multiplying the total drainage area with the average precipitation, $Q_1 = AP$, and (2) by multiplying the total drainage area with the average precipitation added to the substrate uplift rate, $Q_2 = A(P + U)$, to take into account the contribution of eroded sediment. Here A is the upstream drainage area, U the imposed uplift rate and P the precipitation rate.

[13] 3. The channel long profile was constructed from the thalweg elevation at the cross sections.

[14] 4. The local channel geometry was estimated. The channel parameters flow width W, flow depth D, cross-sectional area A_c, wetted perimeter P_w and hydraulic radius R_h were calculated using the continuity equation

$$Q = VA_c, \tag{1}$$

where V is the mean flow velocity. Crucially, this requires the use of an appropriate flow velocity equation. This gives two equations (continuity and velocity), and four independent unknowns (width, depth, cross-sectional area and wetted perimeter), which can be measured from the topography as outlined below. The hydraulic radius is defined as the ratio of cross-sectional area to wetted perimeter.

[15] Because of the extremely small discharge (order of 10^{-3} L/min) it is very difficult to constrain the mean flow velocity equation for the flow directly, either on the experimental surface or in a linear flume. Our attempts to obtain an experimentally determined velocity equation have failed, and instead we have opted for use of existing equations. In our experiments, both Reynolds number ($\mathrm{Re} \approx 10-100$ using the viscosity of pure water) and Froude number ($Fr \approx 10^{-2}-1$) were small, indicating smooth, laminar flow. However, the Weber number, which is the ratio of inertial forces to surface tension ($We = \rho V^2 L/\sigma$, where σ is the surface tension of water), is close to one. This indicates that surface tension is likely to affect the flow velocity. Although good descriptions of flow dominated by surface tension exist in the literature [*Myers et al.*, 2002], they are not easily reduced to a simple velocity equation as required for this study. In fact, *Charpin and Myers* [2005] used the Manning equation to describe the mean flow velocity in a thin film. The Darcy-Weisbach equation, often used to describe turbulent pipe flow, is equivalent to the averaged velocity of laminar flow, and although it does not take surface tension effects into account, it seems the most appropriate available equation. However, the functional dependence of channel parameters on discharge and uplift rate is insensitive to the velocity equation used for analysis (see supplementary material[1]). In this manuscript we present the analysis using two forms of the Darcy-Weisbach equation:

$$V = \sqrt{8g/f}\,R_h^{1/2} S^{1/2}, \tag{2}$$

where g is the gravitational acceleration at the Earth's surface and $f = k_r/\mathrm{Re}$ is a friction coefficient depending on Reynolds number Re and the empirical constant k_r. Using the common definition of $\mathrm{Re} = \rho VL/\eta$, where ρ and η are the density and the viscosity of the fluid respectively and L a typical length scale which is chosen to be the hydraulic radius R_h, the equation can be resolved for V; giving

$$V = K_{DW} R_h^2 S. \tag{3}$$

Here

$$K_{DW} = 8g\rho/k_r\eta \tag{4}$$

is a constant.

[16] As the paste erodes, the silica becomes entrained into the water flow, potentially altering properties such as density and viscosity in a nonnegligible way. We also did calculations including a viscosity term dependent on uplift rate (Appendix A), giving the equation:

$$V = K_{DW}\left(1 + \frac{(1-c)U}{(U+P)}\left(\frac{\rho_s}{\rho_0} - 1\right)\right)\left(1 - \frac{1}{c_p}\frac{(1-c)U}{U+P}\right)^2 R_h^2 S. \tag{5}$$

Here ρ_0 is the density of pure water, c the volume concentration of water in the sediment and c_p the packing density of the sediment.

[17] The friction factor was $k_r = 15$ for the Darcy-Weisbach equation without viscosity variation and $k_r = 12$ for the Darcy-Weisbach equation with viscosity variation by comparing the fit results to a channel with clearly visible banks from experiments on the same set up by *Babault et al.* [2005]. These values are of similar order as values observed for natural rivers.

[18] To extract the channel geometry from the measured topography, we have implemented a routine that varies flow depth within a given cross section of an experimental channel and calculates the corresponding values for width, cross-sectional area, hydraulic radius, wetted perimeter, and flow velocity. The values for which the ratio VA_c/Q is

[1]Auxiliary materials are available in the HTML. doi:10.1029/2005jf000306.

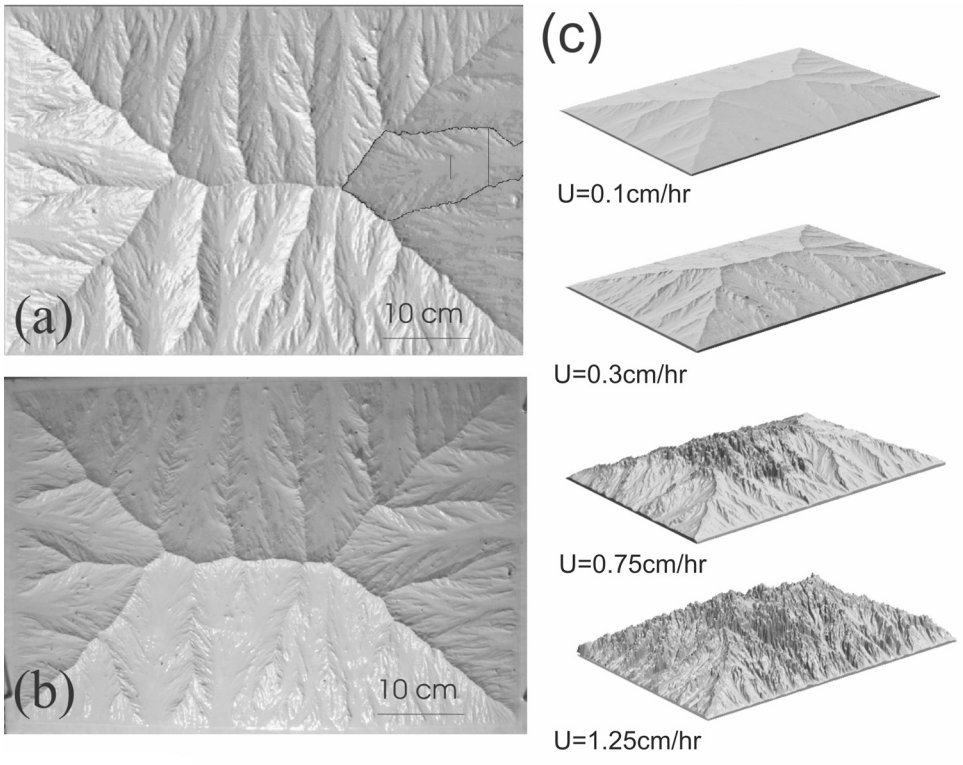

Figure 2. (a) View from above of the DEM of the steady state topography at U = 0.3 cm/hr. The properties of the marked basin are shown in Figure 3. (b) Photograph of the same surface. (c) Oblique view of the DEMs of the experiments of set 2 at uplift rates of 0.1, 0.3, 0.75, and 1.25 cm/hr from top to bottom.

closest to one (with a deviation smaller than 0.1%) are taken as the best fit (see equation (1)).

3. Observations and Results

[19] We have performed three experimental sets, with sets 1 and 2 at a low rainfall rate of 45 mm/hr and set 3 at a high rainfall rate of 140 mm/hr (Table 1). In each set, the topography was allowed to reach a steady state, and data was acquired, before the imposed uplift was changed to a higher rate.

3.1. Topographic Organization

[20] In all experiments, the surface organized into several drainage basins with sizes up to about one tenth of the total system size (Figure 2). The main valleys were evenly spaced, symmetric about the divide and oriented roughly perpendicular to the edge of the erosion box. Once the basins had formed, their outlines changed only slightly over the course of an experiment. *Lague et al.* [2003], *Babault* [2004], and *Babault et al.* [2005] have found similar topographic evolution in earlier experiments and discuss topographic dynamics and steady state characteristics in more detail.

[21] The mean elevation of the experimental surface at steady state increased linearly with the uplift rate (Figure 3a). Differences in this scaling between set 1 and 2, and set 3 are due to precipitation. The steady state mean elevation was lower for set 3 with a rainfall rate of 140 mm/hr than for sets 1 and 2 with a lower rainfall rate of 45 mm/hr. This demonstrates that the erosion rate is dependent on discharge, as higher precipitation rate will increase the discharge at any point of the surface.

3.2. Channels

[22] Unlike earlier experiments by *Crave et al.* [2000], *Lague et al.* [2003], and *Bonnet and Crave* [2003], we have observed channels and channel networks of order 2–3. Channels with a well-defined bank were only observed during the initial development of our experiments from a flat surface and disappeared once the surface was hydraulically fully connected. Similar channels have been observed on and near the fans in the experiments of *Babault et al.* [2005]. After the initial stage, drainage basins with channel networks formed. These channels became progressively more complex and incised as the substrate uplift rate was increased (Figure 2c). The channel cross sections were often not symmetric, with slightly concave walls and a flat floor (Figures 4c and 4d). Channel walls graded into ridge flanks, and without banks, the boundary between the two domains could not be identified directly in the DEMs. Rapid sheet erosion due to high precipitation and runoff prevented the formation of well-defined channels in experiment set 3. The topographies of this set do not meet the requirements of our study. In the following, we focus on results from sets 1 and 2.

3.2.1. Channel Bed Slope

[23] In our experiments, the relationship between the height of the thalweg and the distance to the outlet was linear (Figures 4a and 4b). This relationship is very strong

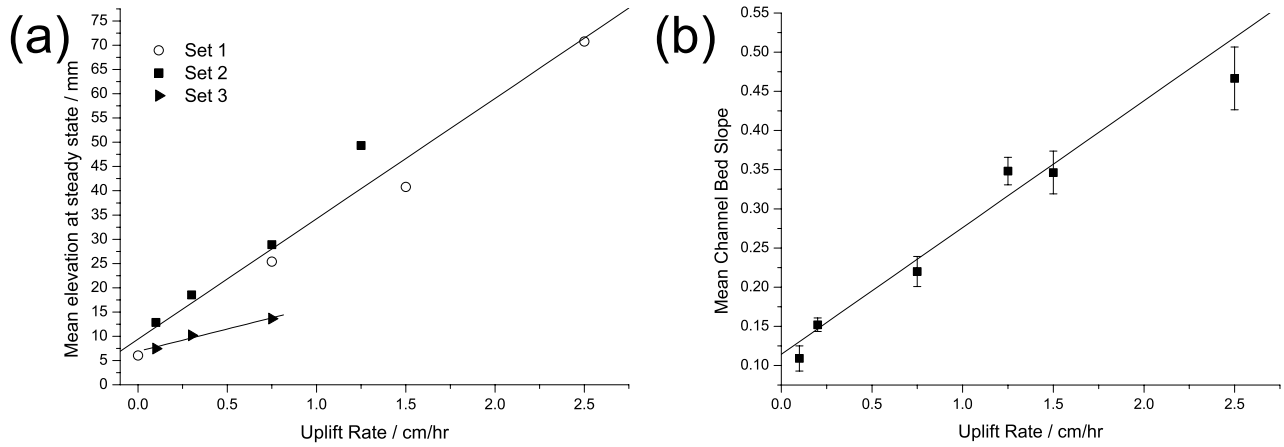

Figure 3. (a) Mean elevation at steady state for all experiments. Circles, set 1; squares, set 2; triangles, set 3. The lines are the best linear fit to the data. (b) Mean channel bed slope averaged over all analyzed catchments at each uplift rate against uplift rate. The solid line represents the best linear fit $S = mU + b$ with $m = 0.16 \pm 0.01$, $b = (11.4 \pm 0.8) \times 10^{-2}$ and $R = 0.98$. Error bars give the standard deviation of the mean.

(the R values of the fits are commonly higher than 0.99), and gives a constant channel bed slope. The few exceptions were due to nonequilibrium features in the basin, such as a propagating knickpoint or blockage due to channel wall failure. For a given uplift rate the channel slope varied little between catchments: the standard deviation of all channel slope measurements in a DEM was usually less than 10% of the mean with only one catchment (at $U = 1.25$ cm/hr) having an exceptionally high slope. The reason for this deviation is unclear. We found that the mean channel slope increases linearly as a function of uplift rate (Figure 3b).

3.2.2. Channel Geometry

[24] Because of the opacity of the experimental set up during rainfall and the small size of topographic features in the erosion box, width and depth of channel flow could not be observed directly. Instead they have been inferred from the cross-sectional geometry of valleys in the DEMs, assuming continuity of flow, as discussed in section 2.3.

[25] The functional form of the downstream relationship between channel width, depth and other channel parameters and discharge is similar for both velocity relations (equations (2) and (5)). For a given discharge, equation (2) gives smaller results than equation (5). Both width and depth do not increase monotonically with discharge in this particular channel. This is mainly due to some fairly large tributaries joining the main channel at various points.

[26] Channel width, depth, cross-sectional area, mean flow velocity, hydraulic radius and wetted perimeter all increase with discharge (Figure 5). *Leopold and Maddock* [1953] and subsequent workers [e.g., *Howard and Kerby*, 1983; *Montgomery and Gran*, 2001; *Snyder et al.*, 2003] observed that many rivers have a geometry that can be described by a power law dependence of width, depth and velocity on discharge. Our experimental results exhibit some scatter, especially for width and wetted perimeter, but a power law model appears to fit our data.

3.2.3. Channel Response to Tectonic Forcing

[27] To find the relationships between the channel parameters and substrate uplift rate we have fitted power laws of the form $B = k_B Q^b$ to the data. B is used in place of any of the calculated channel parameters width W, wetted perimeter P_w, cross-sectional area A_c, flow velocity V, depth D, and hydraulic radius R_h. For the analysis it was assumed that the exponent b is independent of uplift rate. This assumption cannot be deduced from fits where b is optimized as well as k_B, but appears reasonable from the data for all the parameters. Exponents are chosen from the clearest fit values (width and wetted perimeter) or taken to be the average of exponents predicted by linear fits to log-transformed data (depth, cross-sectional area, hydraulic radius, velocity). The exponents used for analysis are presented in Table 3. From the definition of the hydraulic radius we would expect that the powers in the discharge relationship of hydraulic radius and wetted perimeter add up to the power in the relationship of cross-sectional area and discharge. The reported inconsistencies (Table 3) are due to the method of choosing the value for the power described above, rather than arising from inconsistencies within the data. For all channel parameters the prefactor k_B was plotted against uplift rate. Both velocity equations yield almost identical functional forms (Figure 6). Width W, wetted perimeter P_w and cross-sectional area A_c decrease monotonically with increasing uplift rate to a limit value. Fits of exponential decay $k_B = Ae^{-U/U_0} + B_0$ and power law $k_B = B_0 + mU^a$ to the data for W, P_w, and A_c (Figures 7a, 7b, and 7c) both give high R^2 values (Table 4). Here A, a, m, U_0 and B_0 are parameters optimized during regression. Using functions that are decaying to zero do not describe the data as well as functions with a limit value B_0. The mean flow velocity, the hydraulic radius R_h, and the flow depth D (Figures 7d, 7e, and 7f) increase monotonically with uplift rate. In Table 4 we present fit values for the functions on data calculated using the Darcy-Weisbach velocity equation and discharge Q_1.

[28] For the calculations of the channel parameters we have combined the data of sets 1 and 2 for $U = 0.75$ cm/hr. When treated separately, the values for the two sets are very close, with differences within the error limits. For example, for the mean channel bed slope set 1 gives a value of 0.218 ± 0.006 and set 2 0.222 ± 0.014 (errors give

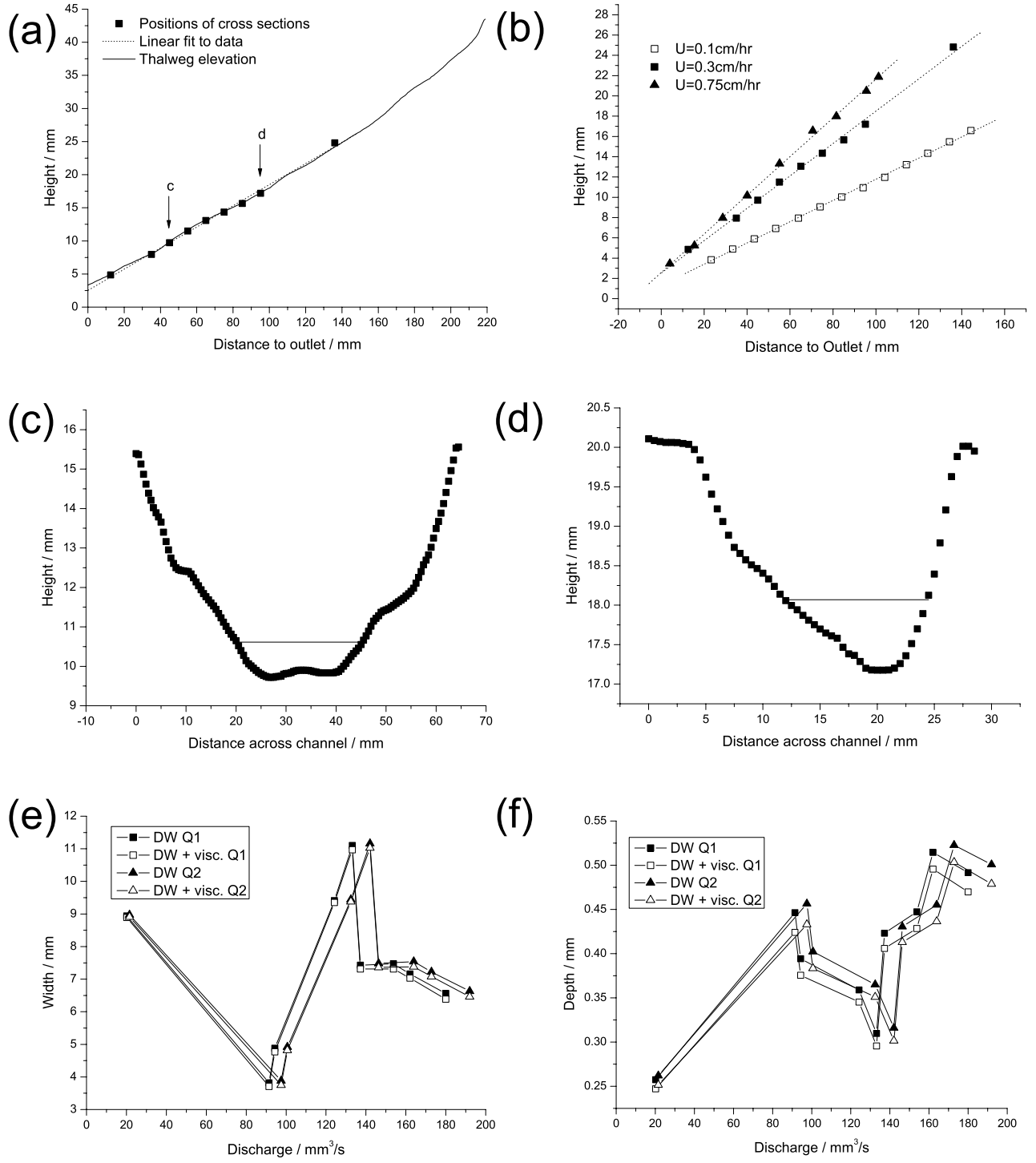

Figure 4. Properties for the catchment marked in Figure 2, at $U = 0.3$ cm/hr. (a) Height at the thalweg against distance to outlet. The squares mark the positions of channel cross section. The solid line gives the thalweg elevation derived with a flow routing algorithm. (b) Height at the thalweg against distance to outlet in the same catchment at three different uplift rates ($U = 0.1$, 0.3, and 0.75 cm/hr). (c and d) Cross sections of the channel with water tables calculated using the Darcy-Weisbach equation and Q_1. The positions of the sections within the catchment are indicated in Figure 2a and are marked in Figure 4a with arrows labeled c and d, respectively. (e) Width values for both velocity equations and discharges Q_1 and Q_2. DW, Darcy-Weisbach; DW + visc, Darcy-Weisbach with varying viscosity. (f) Depth values for both velocity equations and discharges Q_1 and Q_2.

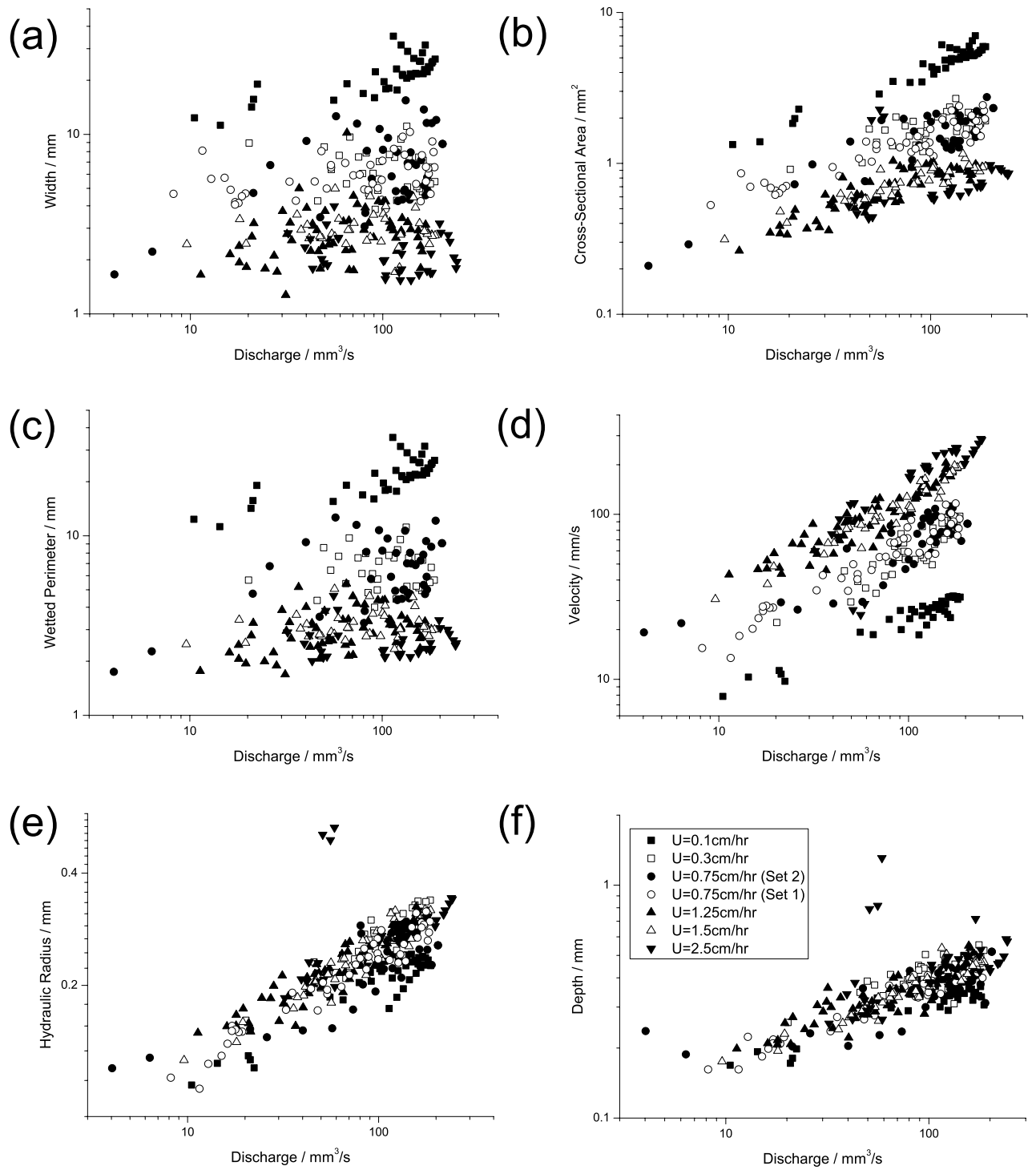

Figure 5. Plots of the channel parameters (a) width, (b) cross-sectional area, (c) wetted perimeter, (d) mean flow velocity, (e) hydraulic radius, and (f) depth against discharge, as calculated using the Darcy-Weisbach velocity equation, separated by uplift rate. The legend for all plots is shown on Figure 5f.

standard error). A similar convergence is found for all geometric channel parameters.

4. Discussion

4.1. On the Nature of Experimental Studies

[29] Working with laboratory-scale experiments as abstraction of geomorphic reality is a matter of tradeoffs. For example in experiments under rainfall, we trade the ability to quantify the flow hydraulics of experimental channels precisely and in real time against a closer qualitative analogy for the realistic interactions between channelized and unchannelized processes. By contrast, in flume experiments [e.g., *Paola et al.*, 1992; *Wohl and Ikeda*, 1997] channel hydraulics are easier to constrain, but flow bound-

Table 3. Values of Powers b in the Power Law $B = k_b Q^b$ Used for the Different Parameters and Velocity Equations Assuming That the Power b is Independent of Uplift Rate

	Equation 2		Equation 5	
	Q_1	Q_2	Q_1	Q_2
W	0.26	0.26	0.26	0.26
A_c	0.42	0.43	0.42	0.43
P_w	0.26	0.26	0.26	0.26
V	0.58	0.57	0.58	0.57
R_h	0.29	0.29	0.29	0.29
D	0.3	0.3	0.3	0.3

aries are often prescribed and hillslope processes are not modeled dynamically. In this study we have strived to optimize the analogy with natural landscapes. The key attribute of our experiments is that the 3D steady state geometry of the channels results from a simplified set of elementary geomorphic processes and is a function of the boundary conditions of the system (substrate uplift and rainfall rate). Unfortunately, experimental constraints (principally the size of the setup) lead to a restricted range of optimum conditions resulting in small channel discharges that are very difficult to measure in situ. We have presented results for two flow resistance equations and possible effects of change in the sediment/water mixture viscosity. Although not explicitly demonstrated in this manuscript, our results are independent of the choice of flow velocity equation (see auxiliary material). Hence even though we actually do not have a single and definitive measure of the width of our channels, we have documented a clear change in the 3D steady state geometry of the channels with changing discharge and incision rate.

4.2. Interpretation of Results

[30] Although our experiments are not scaled models of natural channels, there are several formal analogies: (1) The topography evolves by growth and amalgamation of incisions that spontaneously organize into a drainage network. (2) This drainage network results from the interaction between unchannelized and channelized processes, as well as sediment transport and vertical cutting in the channel. (3) Channel width and depth vary systematically with discharge in a manner qualitatively consistent with natural systems.

[31] Nevertheless, simulation of a natural landscape in a 40×60 cm^2 box results in some discrepancies. Although we do not investigate them in detail in this work, channel statistics such as link length and drainage density seem to differ from what is observed in natural landscapes. In the experimental channels, depth increases faster than width with discharge along the channel; natural streams usually exhibit the opposite [e.g., *Leopold and Maddock*, 1953]. The back calculated flow velocity increases much faster downstream than in natural channels. This is possibly related to the form of the velocity equations used here and/or the insufficient description of the flow hydraulics. Alternatively, it could be related to the concavity of natural channel profiles, since the flow depth decreases with decreasing slope.

[32] We can propose at least two simple experimental incision laws to describe the evolution of the experimental surfaces: (1) a detachment-limited model [*Howard and Kerby*, 1983; *Howard*, 1994; *Whipple and Tucker*, 1999] in which the evolution of the channel is governed by the rate of bed erosion and (2) a transport-limited model [*Smith and Bretherton*, 1972; *Willgoose et al.*, 1991] in which the rate of sediment transport governs the channel evolution. The detailed analysis is presented in Appendix B. For the detachment-limited model, the slope is given by

$$S = \frac{I}{k_e} + \xi_I, \tag{6}$$

where k_e and ξ_I are constants and I is the incision rate. This suggests that a detachment-limited incision law for the channels would be

$$I = k_e(S - \xi_I). \tag{7}$$

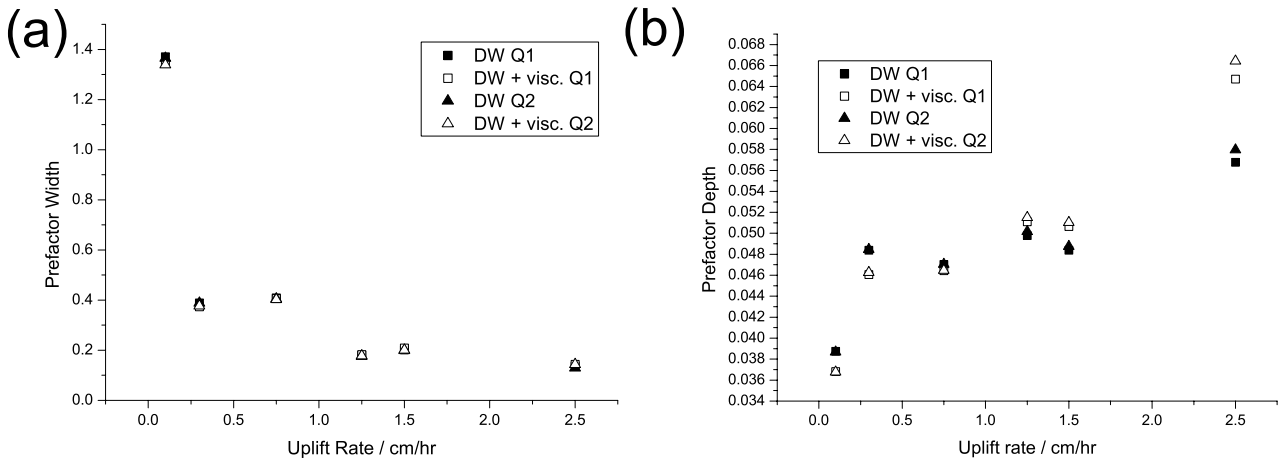

Figure 6. Comparison of width-uplift rate and depth-uplift rate relationships for the different velocity equations and discharges used for the calculation. (a) Prefactor width against uplift rate; (b) prefactor depth against uplift rate. Units of the prefactors differ according to the power used in the relationship with discharge.

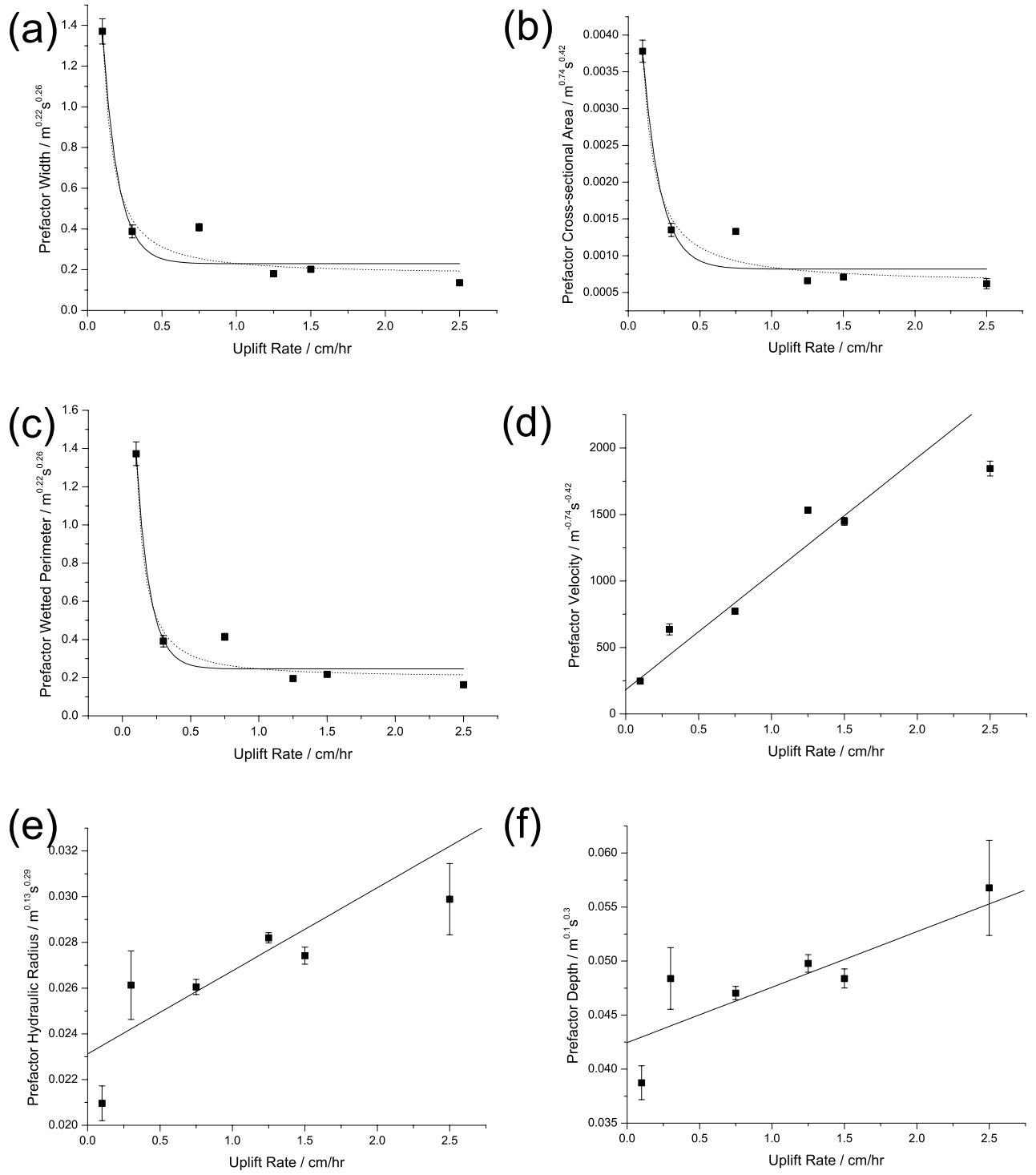

Figure 7. Channel parameters as calculated using the Darcy-Weisbach velocity equation and discharge Q_1 against uplift rate. Error bars give errors in the regression. All fit values are given in Table 4. (a, b, c) Prefactors of width, cross-sectional area, and wetted perimeter against uplift rate. The solid line is the best exponential fit to the data, and the dashed line is the best power law fit. (d, e, f) Prefactors of mean flow velocity, hydraulic radius, and depth against uplift rate. The solid line gives the best linear fit.

[33] In equation (7), ξ_I is the equivalent of a critical slope required to initiate incision. However, because the mean elevation of the experiment is set to a large degree by the slope of the channels, equation (7) does not predict a decrease of mean elevation with precipitation rate as observed in Figure 3a. In a transport-limited model the sediment transport law is given by

$$Q_s = k_s(QS - \xi_Q), \tag{8}$$

Table 4. Fit Values to the Relationships Between Channel Parameters and Uplift Rate[a]

Parameter B Exponential Fit	A	U_0, cm/hr	B_0	R^2
$k_W/m^{0.22}s^{0.26}$	2.99 ± 1.22	0.10 ± 0.04	0.23 ± 0.06	0.96
$k_{Pw}/m^{0.22}s^{0.26}$	3.07 ± 1.28	0.10 ± 0.04	0.25 ± 0.06	0.96
$k_{Ac}/m^{0.74}s^{0.42}$	(6.72 ± 2.29) × 10^{-3}	0.12 ± 0.05	(8.2 ± 1.7) × 10^{-4}	0.96
Allometric fit	m	a	B_0	R^2
$k_W/m^{0.22}s^{0.26}$	(5.2 ± 5.9) × 10^{-2}	−1.36 ± 0.48	0.18 ± 0.08	0.97
$k_{Pw}/m^{0.22}s^{0.26}$	(4.19 ± 5.00) × 10^{-2}	−1.44 ± 0.50	0.20 ± 0.07	0.97
$k_{Ac}/m^{0.74}s^{0.42}$	(1.6 ± 1.1) × 10^{-4}	−1.14 ± 0.29	(6.2 ± 2.5) × 10^{-4}	0.97
Linear fit		m	B_0	R
$k_I/m^{-0.74}s^{-0.42}$		(8.73 ± 0.14) × 10^2	(1.82 ± 0.10) × 10^2	0.97
$k_D/m^{0.1}s^{0.3}$		(5.13 ± 0.96) × 10^{-3}	(4.25 ± 0.10) × 10^{-2}	0.80
$k_{Rh}/m^{0.13}s^{0.29}$		(3.63 ± 0.42) × 10^{-3}	(2.31 ± 0.05) × 10^{-2}	0.84

[a]To obtain the exponential fits, an equation of the form $k_B = Ae^{-U/U0} + B_0$ is used, for the allometric fits the equation $k_B = B_0 + mU^a$ is used, and for the linear fit, $k_B = B_0 + mU$ is used. The constants A and B_0 have the same units as the respective variable k_B; a is dimensionless, and m has units of the corresponding parameter k_B times $(\mathrm{cm/hr})^{-a}$.

where Q_s is the total sediment flux ($=UA$ at steady state) and k_s is a constant and ξ_Q is an erosion threshold proportional to drainage area (Appendix B). Interestingly, equation (8) is equal to the total stream power minus a critical stream power, and predicts a decrease of channel slope with increasing precipitation rate consistent with the relationship observed between mean steady state elevation and precipitation rate. This result suggests that the rate limiting process governing the evolution of the experimental channels is the transport of sediments rather than the rate of bed incision. Intermediate models between detachment and transport-limited conditions could also be tested, but these require studying the transient dynamics of the channels [*Lague et al.*, 2003].

4.3. Comparison With Natural Systems

[34] In the experiments we observed that an increase of the substrate uplift rate results in steepening of the channel slope, narrowing of the channel (to a certain limit) and an increase of the flow velocity paired with only a slight increase of the flow depth. These relationships between channel parameters and uplift rate found in our experiments have parallels in natural systems. At the scale of individual tectonic structures, rivers adjust their channel geometry to tectonic forcing and evolve toward a dynamic equilibrium in which the downward incision matches the uplift of the substrate. The incision at the bed and the erosion of the channel walls are set by a complex relationship between the geometric parameters flow width, depth, the shape of the channel cross section, and the flow velocity. Increasing depth and velocity and decreasing width will increase the shear stress on the channel floor and side and hence the erosion rate, both laterally and vertically. The maximum flow velocity in the cross section is located close to the surface at the center of the flow. Shear stress is proportional to the velocity gradient. This means that larger flow velocity is more effective in increasing the shear stress than a larger flow depth. The channel width will tend to decrease until it reaches a limit where the lateral erosion on the wall is strong enough to counteract any further tendencies to narrow the channel. Our experiments have demonstrated this process, and some recent field studies have reported similar observations. For example, in the Sevier River in southern Utah [*Harbor*, 1998], and rivers draining across the Siwaliks, Nepal [*Lavé and Avouac*, 2001] and the Santa Ynez Mountains, California [*Duvall et al.*, 2004], the channel width decreases with increasing uplift rate, but in none of these cases has a functional relationship been reported. In contrast, *Snyder et al.* [2003] found similar channel widths in nearby segments of the California Coast Range with significantly different rock uplift rates, while many other parameters that are thought to influence channel geometry are constant throughout the area. They proposed various possible reasons for their result, for example effects of changing sediment flux. In light of our experiments another possible explanation is that uplift rates are high enough throughout the area such that the channel width is close to the limit value, in which case this aspect of channel geometry is insensitive to variations in tectonic forcing.

[35] In a detailed analysis of the Bagmati and Bakeya rivers, which are actively cutting through sandstones in the Siwalik Hills of central Nepal, *Lavé and Avouac* [2001] have found that along-stream variations in uplift rate are accommodated either by a change in channel width and slope (Bakeya) as in the experiments, or in channel width only (Bagmati). The different response of the two rivers is possibly due to different discharge characteristics (the Bagmati has about six times the peak discharge of the Bakeya), however, a satisfying explanation has yet to be found.

[36] *Finnegan et al.* [2005] have proposed a model of river width relying on the assumption that the channel width-depth ratio is constant for a given material, or, stated differently, that the channel width is linearly related to the hydraulic radius. The width implicitly depends on incision rate through a power law relationship on channel bed slope. Underlying these premises is the assumption that channel width and depth have the same functional dependence on both discharge and uplift rate, which is not true for the experimental results. The width-depth ratio has a weak dependence on discharge (power law with powers between −0.04 and −0.26; Table 3) and a strong dependence on uplift rate (which can easily be seen from Figure 6). Similar weak dependencies of the width-depth ratio on discharge are seen in natural rivers, although typically the ratio increases downstream. For example, the data of *Leopold and Maddock* [1953] suggest a power law dependence with a power of 0.1.

5. Conclusion

[37] We have performed new laboratory experiments to study the steady state 3D geometry of incising channels as a

function of discharge and incision rate. Channel slope was measured directly but other parameters, such as channel width, depth, cross-sectional area, wetted perimeter, hydraulic radius and flow velocity, had to be estimated using flow velocity equations. We found that channel bed slope is independent of water discharge and increases linearly with increasing substrate uplift rate. The steady state channel width, depth, wetted perimeter, cross-sectional area, hydraulic radius and flow velocity increase with discharge. Width, wetted perimeter and cross-sectional area decrease with increasing substrate uplift rate to a nonzero asymptotic value, which can be described by an exponential decay or a power law. Channel depth and hydraulic radius increase only slightly with uplift rate. As a consequence flow velocity increases significantly with substrate uplift rate. These findings are independent of the flow velocity equation used for the calculations.

[38] Our experiments highlight the importance of both vertical and lateral dynamics of channels in determining their response to tectonic forcing. Provided that an incision law is known, the results suggest that both channel slope and flow width need to be taken into account when calculating fluvial incision rates. Others have reached the same conclusion in the study of natural systems [*Lavé and Avouac*, 2001; *Duvall et al.*, 2004; *Finnegan et al.*, 2005]. Despite some degree of convergence of our experimental results with findings of these field studies, a rigorous comparison of the experiments and natural systems is not possible. It remains unclear when a river adjusts its slope and when it adjusts its width and channel geometry to achieve the required incision.

[39] Even if a direct comparison with natural systems is not possible, we contend that small-scale experiments such as the ones discussed here are a unique opportunity to develop and test our understanding of fluvial erosion and transport processes in well-controlled conditions. In particular, they can help to shed light on the relationships between form and processes at steady state and during transient stages. Moreover, they can be used to validate theoretical models of landscape and channel evolution. If such models cannot quantitatively anticipate the outcome of experiments in a simplified and controlled setting, then it is unlikely that they would produce a better match with natural systems.

Appendix A: Viscosity Dependence on Uplift Rate

[40] To calculate the sediment concentration in the channels at steady state define

$$Q_s = (1-c)UA, \tag{A1}$$

$$Q_w = cUA + PA, \tag{A2}$$

where c is the volume concentration of water in the sediment. The sediment concentration C_{Sed} is then given by the sediment flux Q_s divided by the total flux $Q_w + Q_s$:

$$C_{sed} = \frac{(1-c)U}{U+P}. \tag{A3}$$

In our experiments $c = 0.373$, so the sediment concentration increases approximately linearly with uplift rate and varies between 1.4% and 22.4%. The change of dynamic viscosity with sediment concentration can be described by the Krieger-Dougherty model [*Coussot*, 1997]

$$\eta = \eta_0 \left(1 - \frac{C_{Sed}}{c_p}\right)^{-\lambda c_p} \tag{A4}$$

$c_p = 0.605$ is the packing density, η the viscosity of the mixture and η_0 the viscosity of pure water. λ is the Krieger-Dougherty viscosity coefficient and $\lambda\, c_p = 2$.

[41] This gives a variation function

$$\eta = \eta_0 \left(1 - \frac{(1-c)U}{c_p(U+P)}\right)^{-\lambda c_p}. \tag{A5}$$

The new apparent density is given by

$$\rho = \rho_0 + \frac{(1-c)U}{(U+P)}(\rho_s - \rho_0), \tag{A6}$$

where ρ_0 is the density of pure water. Then the Darcy-Weisbach equation can be written as

$$V = K_{DW}\left(1 + \frac{(1-c)U}{(U+P)}\left(\frac{\rho_s}{\rho_0} - 1\right)\right)\left(1 - \frac{1}{c_p}\frac{(1-c)U}{U+P}\right)^2 R_h^2 S, \tag{A7}$$

with $K_{DW} = 8g\rho_0/k_r\eta$ as before.

Appendix B: Derivation of an Experimental Channel Sediment Transport Law

[42] *Lague et al.* [2003] have shown that a stream power type sediment transport law within a transport-limited framework and a stream power type erosion law within a detachment limited framework can describe the steady state topographic properties of the experimental surfaces. In the transport limited case the sediment flux Q_s is given by

$$Q_s = k_s\left(Q^m S^n - \xi_Q\right), \tag{B1a}$$

for $Q^m S^n > \xi_Q$, where ξ_Q is a transport threshold, and m and n are constants. In the detachment-limited case the erosion rate I is given by

$$I = k_e\left(Q^{m'} S^{n'} - \xi_I\right), \tag{B1b}$$

for $Q^{m'} S^{n'} > \xi_I$, where ξ_I is an erosion threshold, and m' and n' are constants. *Lague et al.* [2003] have shown that the slope of the experimental topographies for discharge Q_1 is given by

$$S = \left(\frac{U}{k_s} + k_\xi\right) P^{-m} A^{1-m}, \tag{B2a}$$

with $k_\xi A = \xi_Q$ for the transport limited case, and

$$S = \left(\frac{U}{k_e} + \xi_E\right) P^{-m'} A^{-m'} \tag{B2b}$$

for the detachment limited case. As the slope is independent of the drainage area in the experiments, m is equal to one and m' is equal to zero. This implies that the slope is independent of precipitation rate for the detachment limited case. Given that the mean elevation in the experimental landscapes is mainly set the channel bed slope, a detachment limited model does not predict the decrease of mean elevation with increasing precipitation rate (Figure 3a) and can be rejected.

[43] For discharge Q_2 the situation is similar. The detachment-limited model can be rejected, while the equivalent of equation (B2a) reads

$$S = \left(\frac{(1-c)U}{k_s} + k_\xi\right)^{\frac{1}{n}} (cU+P)^{-\frac{m}{n}} A^{\frac{1-m}{n}}. \tag{B3}$$

Using $m = 1$, this can be rewritten as

$$S = \left(\frac{(1-c)U}{k_s(cU+P)} + \frac{k_\xi}{(cU+P)}\right)^{\frac{1}{n}}. \tag{B4}$$

Equation (B4) predicts the slope to be approximately linear in U for $n = 1$ and $cU < P$. The highest uplift rate $U = 2.5$ cm/hr gives a value for $cU \approx 0.93$ cm/hr, which is sufficiently smaller than $P = 4.5$ cm/hr.

[44] **Acknowledgments.** We would like to thank J. J. Kermarrec and S. Bonnet for assistance with the experiments and S. Dadson for stimulating discussions. J. Babault kindly provided topographic data of his experiments. K. Whipple, E. Wohl, and three anonymous reviewers helped to improve this work considerably with their comments on earlier versions of the manuscript. We used GridVisual by P. Davy for some of the calculations and visualizations. This work was supported by NERC, the Cambridge Trusts, and CNRS-INSU project RELIEFS.

References

Babault, J. (2004), Dynamique de l'érosion dans une chaıcirc;ne de montagnes: Influence de la sédimentation de piedmont. L'exemple des Pyrénées, Ph.D. thesis, Univ. de Rennes 1, Rennes, France.

Babault, J., S. Bonnet, A. Crave, and J. Van Den Driessche (2005), Influence of piedmont sedimentation on erosion dynamics of an uplifting landscape: An experimental approach, *Geology*, *33*(4), 301–304.

Bonnet, S., and A. Crave (2003), Landscape response to climate change: Insights from experimental modelling and implications for tectonic versus climatic uplift of topography, *Geology*, *31*(2), 123–126.

Charpin, J. P. F., and T. G. Myers (2005), Modelling thin film flow with erosion and deposition, *Adv. Water Resour.*, *28*, 761–772.

Coussot, P. (1997), *Mudflow Rheology and Dynamics*, A. A. Balkema, Brookfield, Vt.

Crave, A., D. Lague, P. Davy, J. Kermarrec, D. Sokoutis, L. Bodet, and R. Compagnon (2000), Analogue modelling of relief dynamics, *Phys. Chem. Earth, Part A*, *25*(6–7), 549–553.

Czirók, A., E. Somfai, and T. Vicsek (1993), Experimental evidence for self-affine roughening in a micromodel of geomorphological evolution, *Phys. Rev. Lett.*, *71*(13), 2154–2157.

Duvall, A., E. Kirby, and D. Burbank (2004), Tectonic and lithologic controls on bedrock channel profiles and processes in coastal California, *J. Geophys. Res.*, *109*, F03002, doi:10.1029/2003JF000086.

Finnegan, N. J., G. Roe, D. R. Montgomery, and B. Hallet (2005), Controls on the channel width of rivers: Implications for modelling fluvial incision of bedrock, *Geology*, *33*(3), 229–232.

Harbor, D. J. (1998), Dynamic equilibrium between an active uplift and the Sevier River, Utah, *J. Geol.*, *106*(2), 181–194.

Hasbargen, L. E., and C. Paola (2000), Landscape instability in an experimental drainage basin, *Geology*, *28*(12), 1067–1070.

Howard, A. D. (1994), A detachment-limited model of drainage basin evolution, *Water Resour. Res.*, *30*, 2261–2285.

Howard, A. D., and G. Kerby (1983), Channel changes in badlands, *Geol. Soc. Am. Bull.*, *94*, 739–752.

Lague, D., A. Crave, and P. Davy (2003), Laboratory experiments simulating the geomorphic response to tectonic uplift, *J. Geophys. Res.*, *108*(B1), 2008, doi:10.1029/2002JB001785.

Lavé, J., and J. P. Avouac (2001), Fluvial incision and tectonic uplift across the Himalayas of central Nepal, *J. Geophys. Res.*, *106*(B11), 26,561–26,591.

Leopold, L. B., and T. Maddock Jr. (1953), The hydraulic geometry of stream channels and some physiographic implications, *U.S. Geol. Surv. Prof. Pap.*, *252*.

Montgomery, D. R., and K. B. Gran (2001), Downstream variations in the width of bedrock channels, *Water Resour. Res.*, *37*, 1841–1846.

Myers, T. G., J. P. F. Charpin, and S. J. Chapman (2002), The flow and solidification of a thin fluid film on an arbitrary three-dimensional surface, *Phys. Fluids*, *14*(8), 2788–2803.

Paola, C., C. Parker, R. Seal, S. K. Sinha, J. B. Southard, and P. R. Wilcock (1992), Downstream fining by selective deposition in a laboratory flume, *Science*, *258*, 1757–1760.

Pelletier, J. D. (2002), Drainage basin evolution in the rainfall erosion facility: Dependence on initial conditions, *Geomorphology*, *53*(1–2), 183–196.

Roering, J. J., J. W. Kirchner, L. S. Sklar, and W. E. Dietrich (2001), Hillslope evolution by nonlinear creep and landsliding: An experimental study, *Geology*, *29*(2), 143–146.

Smith, T. R., and F. P. Bretherton (1972), Stability and the conservation of mass in drainage basin evolution, *Water Resour. Res.*, *8*, 1506–1529.

Snyder, N. P., K. X. Whipple, G. E. Tucker, and D. J. Merritts (2000), Landscape response to tectonic forcing: Digital elevation model analysis of stream profiles in the Mindocino triple junction region, northern California, *Geol. Soc. Am. Bull.*, *112*, 1250–1263.

Snyder, N. P., K. X. Whipple, G. E. Tucker, and D. J. Merritts (2003), Channel response to tectonic forcing: Field analysis of stream morphology and hydrology in the Mendocino triple junction region, northern California, *Geomorphology*, *53*, 97–127.

Whipple, K. X., and G. E. Tucker (1999), Dynamics of the stream-power river incision model: Implications for height limits of mountain ranges, landscape response, and research needs, *J. Geophys. Res.*, *104*(B8), 17,661–17,674.

Whipple, K. X., G. Parker, C. Paola, and D. Mohrig (1998), Channel dynamics, sediment transport, and the slope of alluvial fans: Experimental study, *J. Geol.*, *106*, 677–693.

Willgoose, G., R. L. Bras, and I. Rodriguez-Iturbe (1991), Results of a new model of river basin evolution, *Earth Surf. Processes Landforms*, *16*, 237–254.

Wohl, E., and H. Ikeda (1997), Experimental simulation of channel incision into a cohesive substrate at varying gradients, *Geology*, *25*(4), 295–298.

A. Crave and D. Lague, Géosciences Rennes, UMR 6118, CNRS, Université de Rennes 1, Campus de Beaulieu, CS 74205, F-35042 Rennes Cedex, France.

N. Hovius and J. M. Turowski, Department of Earth Sciences, University of Cambridge, Downing Street, Cambridge CB2 3EQ, UK. (jmt43@esc.cam.ac.uk)